IEEE Access
Multidisciplinary | Rapid Review | Open Access Journal

Received 11 May 2024, accepted 17 June 2024, date of publication 21 June 2024, date of current version 28 June 2024.

Digital Object Identifier 10.1109/ACCESS.2024.3417397

RESEARCH ARTICLE

Model-Free Predictive Control for Improved Performance and Robustness of Three-Phase Quasi Z-Source Inverters

ABDERAHMANE ABID[1], ABUALKASIM BAKEER[2,3], (Senior Member, IEEE), HANI ALBALAWI[4,5], MANSOUR BOUZIDI[6], (Member, IEEE), ABDEREZAK LASHAB[7], (Senior Member, IEEE), ANDRII CHUB[3], (Senior Member, IEEE), AND SHERIF A. ZAID[4]

[1]LEVRES Laboratory, Department of Electrical Engineering, University of El Oued, El Oued 3900, Algeria
[2]Department of Electrical Engineering, Faculty of Engineering, Aswan University, Aswan 81542, Egypt
[3]Department of Electrical Power Engineering and Mechatronics, Tallinn University of Technology, 19086 Tallinn, Estonia
[4]Electrical Engineering Department, Faculty of Engineering, University of Tabuk, Tabuk 47913, Saudi Arabia
[5]Renewable Energy and Environmental Technology Centre, University of Tabuk, Tabuk 47913, Saudi Arabia
[6]Department of Electronics and Communications, University of Ouargla, Ouargla 30000, Algeria
[7]Center for Research on Microgrids (CROM), Aalborg University, 9220 Aalborg, Denmark

Corresponding author: Abualkasim Bakeer (abualkasim.bakeer@aswu.edu.eg)

This work was supported by the Estonian Research Council under Grant PRG2055.

ABSTRACT This paper suggests a novel Model-Free Predictive Control (MFPC) approach for three-phase quasi Z-source inverters (qZSI). While Model Predictive Control (MPC) is popular for qZSI due to its ease of use and performance, it suffers from sensitivity to parameter mismatch. The proposed MFPC overcomes this limitation by relying on an ultra-local model (ULM), eliminating the need for precise parameter matching. This approach establishes a comprehensive mathematical model for key qZSI control variables, including load current, inductor current, and capacitor voltage. Additionally, a unique method seamlessly integrates shoot-through status into the MFPC framework without compromising qZSI operation. Simulation results across various operating conditions demonstrate how much better the suggested MFPC is than the traditional MPC, especially under parameter mismatch scenarios. Notably, the MFPC achieves a significant improvement, exceeding a 37% reduction in total harmonic distortion (THD). Furthermore, the practicality of the proposed MFPC strategy is validated through hardware-in-the-loop (HIL) testing using a C2000TM microcontroller.

INDEX TERMS Ultra-local model, model-free control, model predictive control, parametric uncertainties, quasi Z-source inverter, total harmonic distortion.

I. INTRODUCTION

The Z-source inverter (ZSI) was introduced in 2002 as a viable alternative to the conventional two-level voltage source inverter (VSI). The ZSI employs a Z-source network that consists of two inductors, capacitors, and a diode to perform a buck-boost operation within a converter that operates in a single stage. The ZSI can boost the input voltage to the required DC-link voltage within a single stage by integrating an additional switching state known as the shoot-through (*ST*) state. These features enable the ZSI to deliver enhanced performance, simplified design, and reduced costs [1]. The qZSI, as an advanced and derivative edition of the ZSI, offers some distinct advantages. These include a continuous input current and common ground between the DC supply and the DC-link bus. Furthermore, the voltage across one of the capacitors in the quasi Z-source network is significantly reduced, which leads to a decrease in the size of the passive components [2].

The associate editor coordinating the review of this manuscript and approving it for publication was Tariq Masood.

The qZSI is, therefore, anticipated to have a wide range of applications in sustainable energy systems, including electric vehicle drivetrains [3], photovoltaic applications [4], and energy storage systems [5].

The linear control methods can control the qZSIs efficiently. The primary basic strategies for the qZSI are known as the direct and indirect DC-link voltage control processes. [6]. The cascaded control loops are complicated while obtaining excellent performance because of the simultaneous regulation of the AC and DC sides of the qZSI. Additionally, the DC-side shows evidence of the non-minimum phase system properties [7]. Therefore, other nonlinear control techniques for ZSI/qZSI were proposed, including neural network control [8] and sliding mode control [9]. Such algorithms provide a rapid dynamic response compared to conventional proportional-integral (PI) based controllers but at the expense of a more complicated implementation.

Considering the merits of model predictive control (MPC), such as quick dynamic reaction, easy control structure, and the ability to manage nonlinear features and restrictions, it has been regarded as a potential control solution for the qZSI [10], [11], [12], [13], [14]. The MPC was employed for controlling different qZSI implementations, including the bidirectional qZSI for permanent magnet synchronous machines [10], the H-bridge cascaded multilevel qZSI [11], the neutral-point-clamped qZSI [12], the three-phase four-leg qZSI [13], and the quasi Z-source direct matrix [14].

Numerous techniques have recently been presented to improve the robustness of MPC for various applications in the literature. MPC has two significant challenges: i) resolving the optimization issue requires a substantial number of online computations, and ii) the practicality of MPC is reliant on the accuracy of the system's model. Therefore, the latter could be solved by implementing model-free control that accurately predicts system behavior and enables efficient control actions without relying on a detailed system model. The standard MPC necessitates many computations to solve all the optimization issues online. Various MPC algorithms are presented [15], [16], [17], [18], [19] to reduce the computations of the traditional MPC for the qZSI. A reduced-cost function has been employed for the MPC in [15]. However, simplifying the calculation may compromise the optimization accuracy, leading to suboptimal control performance. In [16], changing the switching state at every switching cycle will lower the current ripple without calculating the cost function. This process may also increase the switching frequency, resulting in increased losses in the power semiconductor devices.

A logical-operational construct for MPC is presented in [17]. The technique uses a sequence of logical representations to eliminate the weighting components and select the vector. However, when employing a single switching vector for the sampling cycle duration, the switching frequency remains variable, leading to a notable current ripple. More empirical evidence is needed to validate its effectiveness. In [20], a discrete-time average MPC approach was implemented for the qZSI. This approach effectively avoided the requirement for loop calculations and cost function evaluations, resulting in enhanced performance at a consistent switching frequency [19]. A proposal is made to employ a vector-based MPC approach to decrease the ripple in the current of the inductor. However, the approach increases the objective function by two weighting parameters, which can jeopardize the technique's computational efficiency. The MPC behavior can be greatly affected by even minor changes in the actual plant dynamics and its representation. Model-free predictive control has become increasingly popular to mitigate this dependency on the system model. MFPC offers advantages similar to predictive control, such as systematically addressing limitations and non-linearities. Additionally, MFPC incorporates a model-free or system-identification approach to reduce reliance on specific characteristics of the system model.

In recent times, the application of MFPC has been explored within the domain of power electronics control. Specifically, it has been investigated for controlling electric motor drives [20] and doubly-fed induction generators [21]. These studies highlight the potential of MFPC in improving control performance and addressing the challenges associated with power electronics applications in various domains. More research in MFPC for DC/AC converters is essential since these MFPC approaches are specifically practical for DC/AC converters [22]. The use of MFPC in drives and power electronics has been reviewed and summarized in the literature [23], which suggests that MFPC strategies are appropriate for addressing rapid dynamics. State-of-the-art approaches have been developed to enable a model-free control approach. These solutions utilize various techniques, such as an ultra-local model (ULM) for predicting future system states [24], a sliding-mode disturbance observer [25], a recursive least squares (RLS) estimator [26], an autoregressive exogenous (ARX) model according to the recursive least squares (RLS) method [22], and a fractional-order controller to define the unknown function of the ULM [27].

This manuscript introduces a novel MFPC technique for qZSI, offering several advantages to cope with the limitations related to the conventional MPC approach. Firstly, the proposed MFPC method can be practical for systems with variable switching frequency, enhancing its versatility. Additionally, it eliminates the need for model parameters, simplifying the control process for qZSI. Furthermore, the detailed development of the integration of shoot-through into the ULM to eliminate dependency on qZSI parameters is presented. This aspect is recognized as a challenge for qZSI. The study also evaluates the behavior of the qZSI using traditional MPC to benchmark it against the proposed MFPC. The findings illustrate the efficacy and superiority of the proposed MFPC technique, particularly in situations characterized by dynamic operational settings and scenarios featuring parameter mismatches. The main findings of the paper can be summarized as follows:

- Propose a robust algorithm for predictive control of qZSI, addressing parameter mismatches within the model.
- The control input required by the ULM to estimate the unknown function is determined by considering the unique state of the shoot-through in the qZSI. This task is deemed challenging compared to the existing MFPC approaches found in the literature.
- Thoroughly benchmarking the proposed MFPC against conventional MPC for qZSI, elucidating key differences and performance metrics.
- The simulation findings demonstrate the feasibility of the suggested MFPC procedure in reducing the THD in the load current, while also showcasing its immunity to parameter mismatches when compared to traditional MPC.
- Validation of the suggested MFPC through HIL testing.

The remaining parts of the manuscript are structured in the following manner: Section II presents the traditional MPC approach designed for the qZSI. However, in Section III, the proposed MFPC algorithm is comprehensively explained. The simulation findings, showcasing the performance and effectiveness of the suggested MFPC method, are displayed in Section V. Section IV validates the advantages of the suggested MFPC method employing HIL validation. The comparative investigation is illustrated in Section VI. After all, Section VII provides a conclusion to the paper by reviewing the findings and implications of the study.

II. CONVENTIONAL MPC CONTROL OF qZSI

The qZSI is a single-stage DC/AC power converter that utilizes a unique impedance network to boost the output voltage. The qZSI power circuit is presented in Figure 1. It contains a DC supply, a quasi-Z-source network (qZSN), a 3-ϕ inverter, and a three-phase *RL* load. The generation of the desired output voltage is achieved through the amalgamation of active and null voltage vectors, accompanied by the integration of an additional *ST* state into the space vector diagram (SVD). As a result, there are eight essential voltage vectors for the qZSI, seven of which are used in non-*ST* states and one in the *ST* state.

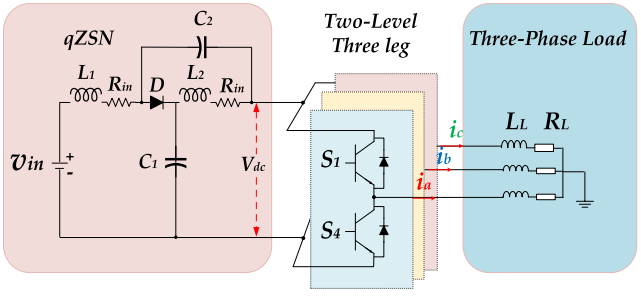

FIGURE 1. Three-phase qZSI topology.

MPC can be applied to the qZSI to improve its performance by predicting switching states, optimizing the control inputs, and ensuring the system remains within safe operating limits. Implementing conventional MPC in the qZSI involves the following steps: i) The first one is known as prediction, and it measures variables such as 3-ϕ currents, inductor current, and capacitor voltage. ii) The next stage is to predict the future value of the variables, which are determined from actual measurements. iii) The third part is optimization; it picks the appropriate switching state corresponding to the lowest objective function value.

The control architecture of the system is significantly simplified when MPC is implemented on the qZSI. As presented in Figure 2, the instantaneous output 3-ϕ current (i_a, i_b, and i_c) transformed into $\alpha\beta$ coordinates (i_α and i_β) at the present point are first sampled to predict their states for the next sampling cycle. After that, the defined objective function is evaluated according to the predicted control variables and their reference values to reach an optimum output voltage vector that can achieve a good control performance of the inductor current, output currents, and capacitor voltage. The optimum voltage vector is transformed into the switching state of the inverter as part of the control of the qZSI. This procedure allows for controlling and manipulating the qZSI's functioning effectively.

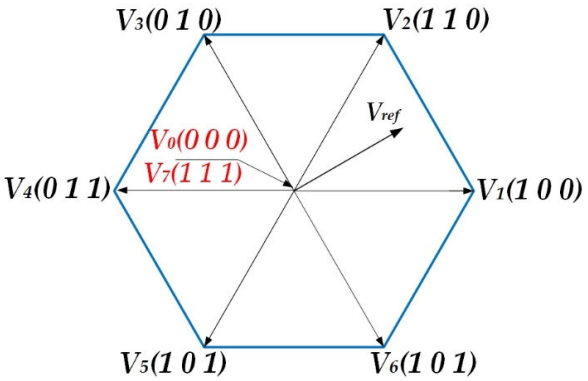

FIGURE 2. Voltage space vector representation for qZSI.

A. INVERTER LOAD CURRENTS PREDICTION MODEL

To incorporate the output currents as control variables, their actual values are measured and fed back into the control loop. The output currents are converted into the stationary frame (α, β), as seen in Figure 2. This conversion allows for further analysis and manipulation of the currents within a fixed reference frame. As shown in Table 1, the 3-ϕ inverter features eight switching states (S_0– S_7) with defined $\alpha\beta$ voltage vector values. The Clark transformation is utilized to convert the output currents (i_{abc}) in a 3-ϕ system, typically expressed in the *abc* coordinate framework, into the $\alpha\beta$ coordinate system (1).

$$\begin{bmatrix} x_\alpha \\ x_\beta \end{bmatrix} = T_{\alpha\beta/abc} \begin{bmatrix} x_a \\ x_b \\ x_c \end{bmatrix},$$

where

$$T_{\alpha\beta/abc} = \sqrt{\frac{2}{3}} \begin{bmatrix} 1 & -1/2 & -1/2 \\ 0 & \sqrt{3}/2 & -\sqrt{3}/2 \end{bmatrix} \quad (1)$$

TABLE 1. qZSI voltage vectors.

		Switching states							Voltage vector	
	j	V_j	S_1	S_2	S_3	S_4	S_5	S_6	V_α	V_β
Non-ST	0	V_0	0	0	0	1	1	1	0	0
	1	V_1	1	0	0	0	1	1	$2V_{dc}/3$	0
	2	V_2	1	1	0	0	0	1	$V_{dc}/3$	$\sqrt{3}V_{dc}/3$
	3	V_3	0	1	0	1	0	1	$-V_{dc}/3$	$\sqrt{3}V_{dc}/3$
	4	V_4	0	1	1	1	0	0	$-2V_{dc}/3$	0
	5	V_5	0	0	1	1	1	0	$-V_{dc}/3$	$-\sqrt{3}V_{dc}/3$
	6	V_6	1	0	1	0	1	0	$V_{dc}/3$	$-\sqrt{3}V_{dc}/3$
ST	7	V_7	1	1	1	1	1	1	0	0

Here, $T_{\alpha\beta/abc}$ denotes the Clark matrix transformation, where 'x' symbolizes the voltage and current variables.

Figure 2 depicts the SVD and illustrates the various space vector representations of the output voltages between the load terminals, as given by the discrete-time equation:

$$V_p(k+1) = 2V_{dc}(S_1 + aS_2 + a^2S_3)\Big/3 \tag{2}$$

where $p = (0 \text{ to } 7)$, V_{dc} is the maximum value for the DC-bus voltage, $a = e^{j2\pi/3}$ and S_1, S_2, and S_3 are the upper switching states for legs a, b, and c, respectively.

When considering a three-phase inductive load (RL) at the output of the qZSI, the following may be used to determine the output voltage in the $\alpha\beta$ plane:

$$V_{(\alpha,\beta)} = L\frac{di_{(\alpha,\beta)}}{dt} + Ri_{(\alpha,\beta)} \tag{3}$$

In the $\alpha\beta$ plane, the output currents are denoted by i_α and i_β.

The following discrete-time equation can describe the differential of the output current using Euler's procedure:

$$\frac{di_{(\alpha,\beta)}(k)}{dt} = \frac{i_{(\alpha,\beta)}(k) - i_{(\alpha,\beta)}(k-1)}{T_S} \tag{4}$$

In the given context, the indices k and k-1 designate the current and previous sampled values, respectively, when referring to the current and control values. To calculate the upcoming estimate of the output currents, the time is advanced by one sampling cycle, as shown below:

$$i_{(\alpha,\beta)}(k+1) = \frac{T_S V_{(\alpha,\beta)}(k+1) + L\, i_{(\alpha,\beta)}(k)}{RT_S + L} \tag{5}$$

B. CAPACITOR VOLTAGE AND INDUCTOR CURRENT PREDICTION MODELS

Figures 3 and 4 illustrate the circuits that describe the qZSI's operating modes. In the non-*ST* mode, the inductors L_1 and L_2 absorb power from the input as well as the capacitors C_1 and C_2. Meanwhile, the inductors will feed the capacitors in *ST* mode. Therefore, to accurately predict the behavior of the inductor current i_{L1} and the capacitor voltage v_{C1}, it is necessary to develop prediction models specific to the operating mode of the qZSI. These prediction models will consider the unique characteristics and dynamics of the qZSI

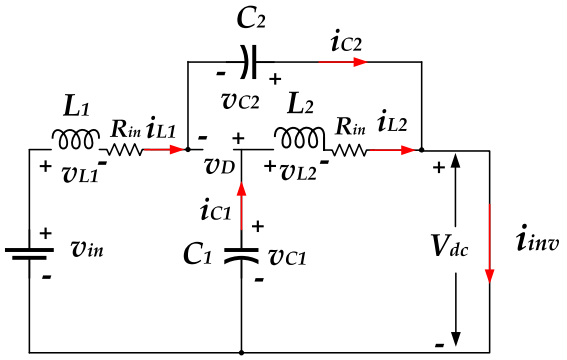

FIGURE 3. The qZSI power circuit in non-*ST* mode.

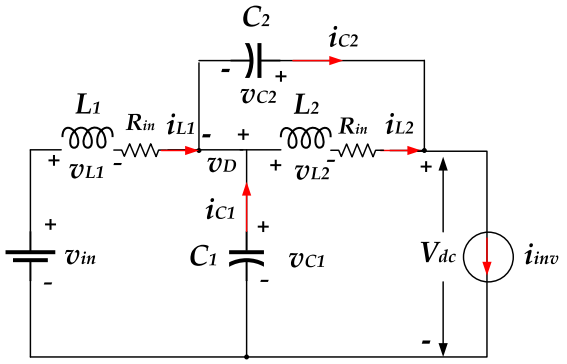

FIGURE 4. The qZSI power circuit in *ST* mode.

in each operating mode to ensure accurate and reliable i_{L1} and v_{C1} predictions.

C. NON-ST MODE

As depicted in Figure 3, the non-*ST* state of the qZSI, encompassing both zero and active modes, can be characterized mathematically by the following equations that describe the voltage across capacitor C_1 and the current passing via inductor L_1:

$$C_1\frac{dv_{C1}(k)}{dt} = i_{L1}(k) - i_{inv}(k) \tag{6}$$

$$L_1\frac{di_{L1}(k)}{dt} = v_{c1}(k) - v_{in}(k) + R_{ind}\, i_{L1}(k) \tag{7}$$

where C_1 is the capacitance, L_1 is the inductance of the qZSN; R_{ind} is the equivalent series resistance of the inductor, v_{in} and v_{C1} are the DC source and capacitor C_1 voltages, respectively; i_{L1} is the current via inductor L_1, during the k^{th} instant.

The i_{inv} is the output current of the qZSI, which may be resolved by the switching state procedure described below:

$$i_{inv}(k) = S_1 i_a(k) + S_2 i_b(k) + S_3 i_c(k) \tag{8}$$

In (8), $i_a(k)$, $i_b(k)$, and $i_c(k)$ are the discrete 3-ϕ output currents. It is noteworthy that when the qZSI functions in the null state, $i_{inv}(k)$ equals zero. This means that the current flowing through the inverter (i_{inv}) is zero during the null state of the qZSI operation.

The predicted i_{L1} and $v_{C1}$are derived by using Euler's procedure to discrete (6) and (7) as follows:

$$i_{L1}(k+1) = \frac{T_S(v_{in}(k) - v_{C1}(k)) + L_1 i_{L1}(k)}{L_1 + R_{ind} T_S} \quad (9)$$

$$v_{C1}(k+1) = v_{C1}(k) + \frac{T_S}{C_1}(i_{L1}(k+1) - i_{inv}(k+1)) \quad (10)$$

D. NON-ST MODE

In Figure 5, when the diode is switched off, all of the capacitors immediately evacuate the stored energy into the inductors upon reaching the *ST* state. The following equations might be employed to explain the voltage across an inductor and the current via a capacitor in this specific case:

$$L_1 \frac{di_{L1}(k)}{dt} = v_{C1}(k) + R_{ind}\, i_{L1}(k) \quad (11)$$

$$C_1 \frac{dv_{c1}(k)}{dt} = -i_{L1}(k) \quad (12)$$

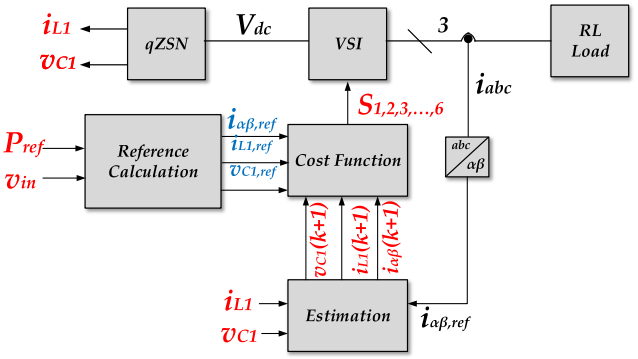

FIGURE 5. Diagram of the proposed MFPC for qZSI.

According to Euler's procedure, (11) and (12) are discretized to determine the future capacitor voltage and inductor current, which are described as:

$$i_{L1}(k+1) = \frac{T_S v_{C1}(k) + L_1 i_{L1}(k)}{L_1 + R_{ind} T_S} \quad (13)$$

$$v_{C1}(k+1) = v_{C1}(k) - \frac{T_S}{C_1} i_{L1}(k+1) \quad (14)$$

E. OBJECTIVE FUNCTION OF THE TRADITIONAL MPC

The preceding qZSI model (see (11)-(14)) is used in conjunction with the conventional MPC approach to forecasting the system's future behavior, including the i_{L1}, v_{C1}, and i_{abc}. Using this predictive model, a cost function defined in (15) is established and evaluated to determine the optimum voltage vector for every sampling period. The objective function is critical in determining the optimal control action, as it assesses and chooses the most advantageous alternative by considering the predicted behavior of the system.

$$g = \left|i_{\alpha,ref} - i_{\alpha}(k+T_S)\right| + \left|i_{\beta,ref} - i_{\beta}(k+T_S)\right| + \lambda_C \left|v_{C1,ref} - v_{c1}(k+T_S)\right| + \lambda_L \left|i_{L1,ref} - i_{L1}(k+T_S)\right| \quad (15)$$

In (15), the symbols λ_L and λ_C denote the weighting parameters assigned to the current through the inductor L_1 and the voltage across the capacitor C_1, respectively. $i_{\alpha,ref}$ and $i_{\beta,ref}$ denote the reference current components in the $\alpha\beta$ plane, while $i_{L1,ref}$ and $v_{C1,ref}$ represent the reference values for the inductor current and capacitor voltage, respectively. These parameters play a crucial role in shaping the objective function and influencing the control decisions made by the MPC algorithm.

III. PROPOSED MODEL-FREE PREDICTIVE CONTROL FOR qZSI

The key objective of the control system for the qZSI is to cancel the errors between the reference values and their measured variables (i_{L1}, v_{C1}, $i_{\alpha\beta}$). This is achieved by employing a cost function such as (15). In the instance of the traditional MPC, the output current predictions are calculated using the load resistance and inductance knowledge on the AC side. Moreover, the capacitor voltage and inductive current are computed using the capacitance and inductance values associated with the qZSI. Thus, any uncertainty in the model produces inaccurate current and voltage predictions, reducing the performance of MPC for qZSI.

The inspiration behind the proposed MFPC is to decrease the information in the framework required to perform forecasts and compute ideal control activities as much as possible. To achieve this, a mathematical demonstration with a standard structure is chosen so that negligible past information about the physical framework is required. At that point, by utilizing an estimation calculation, the parameters of the model are consequently upgraded utilizing input and output estimations. Figure 5 depicts the schematic representation of the proposed MFPC approach.

The prediction demonstrated in Figure 6 is built expecting detailed information about the physical framework to be accessible and time-invariant, and its execution is influenced in the event that this assumption is not satisfied. Conversely, the proposed controller employs an estimation approach to detect changes in the physical system's parameters or unmodeled behavior. The cost function in the proposed MFPC retains the same terms as the conventional MPC, but with a modification specifically, the error terms are squared, as illustrated below:

$$g = \left(i_{\alpha,ref} - i_{\alpha}(k+1)\right)^2 + \left(i_{\beta,ref} - i_{\beta}(k+1)\right)^2 + \lambda_C \left(v_{C1,ref} - v_{C1}(k+1)\right)^2 + \lambda_L \left(i_{L1,ref} - i_{L1}(k+1)\right)^2 \quad (16)$$

However, a key distinction lies in the treatment of error terms. Unlike MPC, which might use the absolute value or linear terms for errors, the MFPC cost function incorporates squared error terms. Due to the squared error, terms can be increased emphasizing large errors and simplified optimization for the proposed MFPC.

When using the estimated load model for a certain inverter voltage vector, the real and imaginary components of the

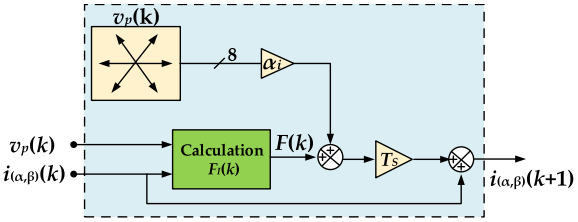

FIGURE 6. Block diagram of the ULM AC side-based MFPC.

load current vector are estimated as $i_\alpha(k+1)$ and $i_\beta(k+1)$, respectively, for determining the optimal voltage vector in the next sampling period. In the same way, $v_{C1}(k+1)$ and $i_{L1}(k+1)$ are estimated as the capacitor voltage and inductive current using the proposed estimation of the qZSI parameters. The following subsections detail the estimation method.

A. PREDICTION MODEL OF THE CAPACITOR VOLTAGE AND INDUCTOR CURRENT

1) AC PART DISCRETE-MODEL

In the proposed MFPC technique, the estimation of future output current relies on the current variations detected by the ultra-local model (ULM). As described in [28], the ULM of a single-input single-output (SISO) system can be modeled as a first-order system, characterized by its dynamics and input-output relationship and can be modeled as

$$\frac{dY(t)}{dt} = F(t) + \alpha U(t) \tag{17}$$

where $Y(t)$ denotes the system's outputs, whereas $F(t)$ represents the system's attributes, known and unknown, including disturbances. The constant α, which is a nonphysical constant, is utilized to alter the sequence of the inputs in (17).

The value of α is typically determined through trial and error, allowing for fine-tuning of the input in order to optimize the system's performance. When comparing (17) with (3), it is possible to derive the model of the qZSI based on the ULM.

$$\frac{di_{(\alpha,\beta)}(t)}{dt} = F_I(t) + \alpha_i v_p(t) \tag{18}$$

where α_i is a nonphysical constant for the load current term, and $v_p$is the qZSI voltage vector and system input. The current variations associated with the qZSI's eight voltage vectors may be computed using the first-order discrete-time ULM in (17), as shown below:

$$\Delta i_{(\alpha,\beta)}(k) = T_S(F_I + \alpha_i v_p(k)), p = 0, \ldots, 7 \tag{19}$$

The output current prediction model is determined by considering the variations in the output current ($\Delta i_{\alpha,\beta}(k)$) between the $(k+1)$ and (k) sampling periods. The model considers the eight voltage vectors of the inverter, as defined in Table 1. By analyzing the current variations and incorporating the voltage vectors, the model enables an accurate prediction of the output current behavior in subsequent sampling periods as:

$$i_{(\alpha,\beta)}(k+1) = i_{(\alpha,\beta)}(k) + T_S(F_I + \alpha_i v_p(k)) \tag{20}$$

Figure 5 represents the block diagram of the ULM-based MFPC for the AC side. This diagram provides an overview of the control system, showcasing the relationship between different components and modules involved in the MFPC algorithm. It serves as a visual representation of how the ULM is utilized in conjunction with the MFPC approach to achieve effective control over the AC side of the system.

2) DC PART DISCRETE-MODEL

The Euler backward technique is used to transform the converter state variables' derivatives to the discrete-time analysis form:

$$\begin{bmatrix} i_{L1-ST}(k+1) \\ i_{L1-nST}(k+1) \\ v_{C1-ST}(k+1) \\ v_{C1-nST}(k+1) \end{bmatrix} = \begin{bmatrix} F_{L1-ST} + \alpha_{ST} i_{inv} \\ F_{L1-nST} + \alpha_{nST} i_{inv} \\ F_{C1-ST} + \alpha_{ST} i_{inv} \\ F_{C1-nST} + \alpha_{nST} i_{inv} \end{bmatrix} T_S + \begin{bmatrix} i_{L1-ST}(k) \\ i_{L1-ST}(k) \\ v_{L1-ST}(k) \\ v_{L1-ST}(k) \end{bmatrix} \tag{21}$$

3) DETERMINATION OF THE UNKNOWN FUNCTION F

The estimated value of the unknown function F can be obtained by applying algebraic identification methods. It is expected that F can be accurately estimated, which results in $F = \hat{F}$. The estimated value of $\hat{F}$ is calculated as follows for every iteration:

$$\hat{F} = -\frac{3}{j^3 T_S} \sum_{h=1}^{j} \left(\hat{F}_1 + \hat{F}_2 \right) \tag{22}$$

where

$$\hat{F} = -\frac{3}{j^3 T_S} \begin{bmatrix} \hat{F}_i & \hat{F}_{L1-ST} & \hat{F}_{L1-nST} & \hat{F}_{C1-ST} & \hat{F}_{C1-nST} \end{bmatrix}^T,$$

and j,h are the window sequence dimensions, while $\hat{F}_1$and$\hat{F}_2$ can be obtained from (23) and (24), as shown at the bottom of the next page, respectively. where α, α_{ST}, α_{nST} are the constant coefficients of the AC side, the DC side for the *ST*, and non-*ST* states, respectively. The calculation of $v_{C1-ST}(k+1)$, $i_{L1-ST}(k+1)$, v_{C1-nST} $(k+1)$, and $v_{C1-ST}(k+1)$ can be explain in Figures 7 and 8.

Figure 9 illustrates the flowchart of selecting the appropriate switching states for each sampling time in the proposed MFPC of qZSI. In the first stage, the proposed algorithm measures the i_{abc}, v_{C1}, and i_{L1}. Then, the procedure applies the Clarke transformation to the 3-ϕ output currents. The predicted output current of the proposed MFPC algorithm is computed based on the equations presented in Figure 7 and Eq. (20). The procedure is started by adjusting the optimum objective function (g_{opt}) before entering the control loop. The predicted values for v_{C1} and i_{L1} are determined using the technique in Figures 7 and 8 considering all states and all vectors. In order to begin the optimization process, the controller essentially determines the cost function using (16).

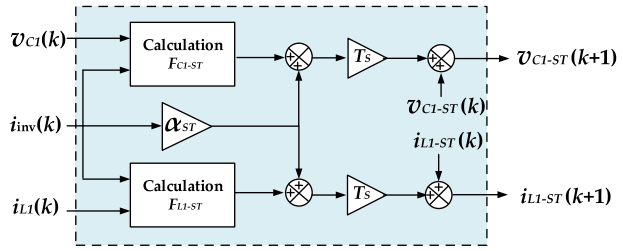

FIGURE 7. Structure of proposed MFPC in *ST* state.

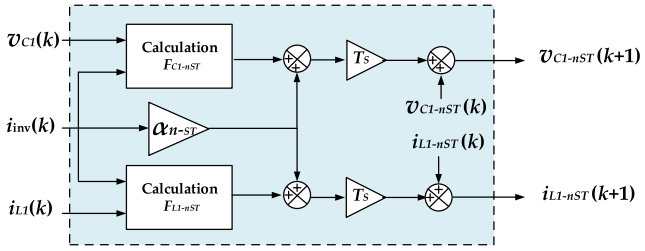

FIGURE 8. Structure of the proposed MFPC in non *ST* state.

Based on the optimized cost function value, MFPC chooses the appropriate switching state that corresponds to the best control action. This process ensures efficient optimization and determines the optimal switching state for the qZSI.

4) REFERENCES CALCULATIONS

Several factors are taken into account when defining the value of $v_{C1,ref}$ and $i_{L1,ref}$ values. The reference $i_{L1,ref}$ is estimated based on the desired output power to be injected into the RL load, as specified in (25).

$$i_{L1}(k) = P_{ref} \big/ v_{i_n}(k) \tag{25}$$

This estimation ensures the inductor current is appropriately adjusted to meet the system's power requirements. On the other hand, it is established that v_{C1} must be at least twice the value of the peak phase voltage to provide required line-to-line voltages. This requirement ensures that the capacitor voltage remains sufficiently high to support the operation of the qZSI and maintain stability. The system can adequately handle voltage fluctuations and maintain reliable performance by setting the capacitor voltage at this level.

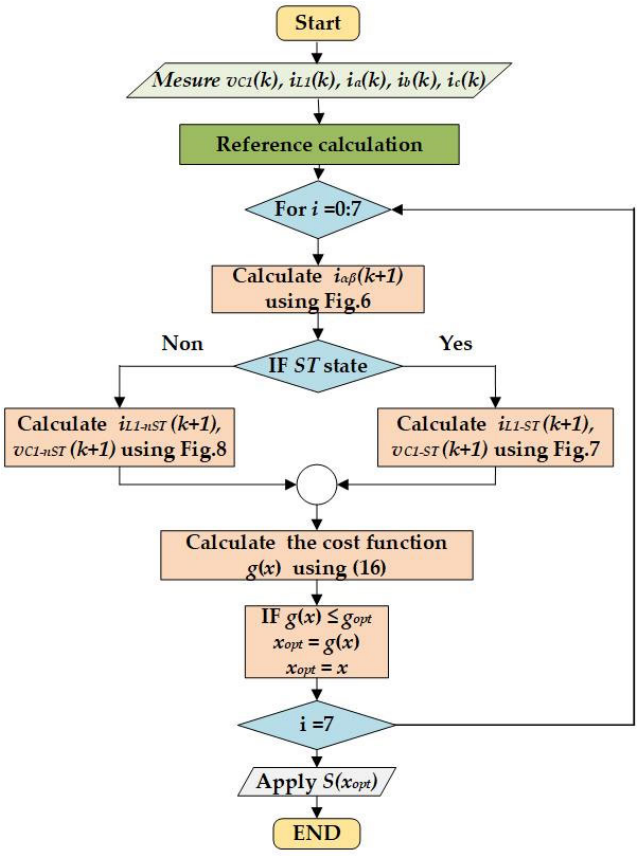

FIGURE 9. Flowchart of the proposed MFPC for qZSI.

The reference of the output current $\alpha\beta$ plane is represented as follows

$$\left[i_{\alpha,ref}\ i_{\beta,ref}\right]^T = T_{\alpha\beta/abc}\sqrt{\frac{2P_{ref}}{3R}}\left[i_{a,ref}\ i_{b,ref}\ i_{c,ref}\right]^T \tag{26}$$

In this context, R refers to the load resistance, while P_{ref} denotes the active power load reference. The equation relates these elements to define the reference for the output current in the $\alpha\beta$ plane. This reference current, when applied through appropriate control strategies, helps achieve

$$\hat{F}_1 = \begin{bmatrix} (j-2(h-1))i_\alpha(k-1) + (j-2h)i_\alpha(k) \\ (j-2(h-1))i_\beta(k-1) + (j-2h)i_\beta(k) \\ (j-2(h-1))i_{L1-ST}(k-1) + (j-2h)i_{L1-nST}(k) \\ (j-2(h-1))i_{L1-nST}(k-1) + (j-2h)i_{L1-ST}(k) \\ (j-2(h-1))v_{C1-ST}(k-1) + (j-2h)v_{C1-ST}(k) \\ (j-2(h-1))v_{C1-nST}(k-1) + (j-2h)v_{C1-nST}(k) \end{bmatrix} \tag{23}$$

$$\hat{F}_2 = \begin{bmatrix} \alpha(h-1)T_S(j-(h-1))v_\alpha(k-1) + \alpha\, iT_S(j-h)v_\alpha(k) \\ \alpha(h-1)T_S(j-(h-1))v_\beta(k-1) + \alpha\, iT_S(j-h)v_\beta(k) \\ \alpha_{ST}(h-1)T_S(j-(h-1))i_{inv}(k-1) + \alpha_{ST}iT_S(j-h)i_{inv}(k) \\ \alpha_{nST}(h-1)T_S(j-(h-1))i_{inv}(k-1) + \alpha_{nST}iT_S(j-h)i_{inv}(k) \\ \alpha_{ST}(h-1)T_S(j-(h-1))i_{inv}(k-1) + \alpha_{ST}iT_S(j-h)i_{inv}(k) \\ \alpha_{nST}(h-1)T_S(j-(h-1))i_{inv}(k-1) + \alpha_{nST}iT_S(j-h)i_{inv}(k) \end{bmatrix} \tag{24}$$

TABLE 2. Specifications of the system.

Circuit parameters	Value
$C_{1,2}$, $L_{1,2}$	2.5 mF, 4 mH
Internal resistance r_c, R_{in}	0.19 Ω, 0.1 Ω
Three-phase load L, R	24 mH, 12 Ω
Sampling time Ts	20 µs
Input voltage v_{in}	100 V
Output frequency f	50 Hz
Output voltage	142 V

the desired active power transfer and regulates the system's behavior.

IV. SIMULATION RESULTS

In order to assess and verify the efficacy of the proposed MFPC approach depicted in Figure 5, a comparative simulation analysis is carried out using MATLAB/Simulink. The conventional MPC and the proposed MFPC were simulated and compared. The comparison between these control strategies was based on their respective abilities to achieve accurate tracking, reject disturbances, and maintain robustness in the face of variations in system parameters. The simulation models incorporate various parameters listed in Table 2 before entering the control loop. These factors greatly influence the performance and behavior of the control techniques. A prediction horizon of $k + 2$ is considered for the MFPC algorithms to mitigate the computational delay effect. A dependable and effective control strategy is ensured by selecting a prediction horizon that balances computing effort and forecast accuracy.

A. SCENARIO 1: TRANSIENT PERFORMANCE OF THE SUGGESTED MFPC AND THE TRADITIONAL MPC

When a step change in the output reference current occurs, the transient performance of the suggested MFPC and traditional MPC algorithms is evaluated. The obtained results are presented in Figures 10 and 11, respectively. These figures illustrate the behavior of the dc-link voltage, capacitor voltage, inductive current, three-phase load current, the error between the measured and reference output phase current, and the harmonic spectrum for the output current after the transient response of the proposed MFPC and traditional MPC, respectively.

The two controllers measure the signals of i_{abc}, v_{C1}, and i_{L1} as feedback. In this case study, at the instant t= 200 ms, the required output power P_{ref} is increased from 500 W to 800 W, and the associated steady-state references are modified according to (25). As a result, the i_{L1} reference increases from 5 A to 8 A, and the output current increases from 5.7 A to 7.3 A.

Regarding the DC-link voltage, the proposed MFPC approach maintains the voltage unchanged under the step change, as depicted in Figure 10(a), while the conventional approach exhibits increased voltage ripple as shown in Figure 11(a). It is worth noting that the proposed MFPC

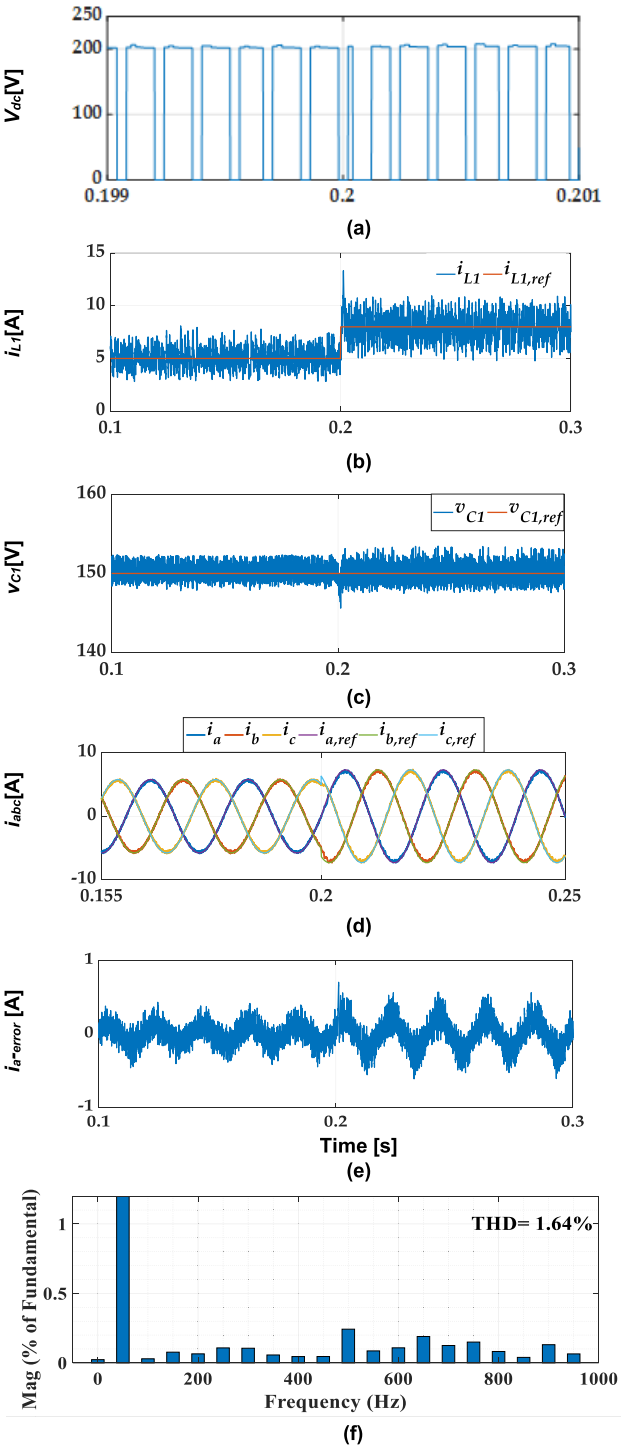

FIGURE 10. Simulation results for the proposed MFPC of qZSI.

introduces a higher ripple in the current of the inductor L_1, which can be attributed to the variation in switching frequencies, as seen in Figures 10(b) and 11(b).

Meanwhile, as shown in Figures 10(c) and 11(c), the capacitor voltage maintains a constant at 150 V under the step change. In both cases, the i_{abc} accurately follows the sinusoidal references, as shown in Figures 10(d) and 11(d). Moreover, in Figures 10(e) and 11(e) the proposed MFPC

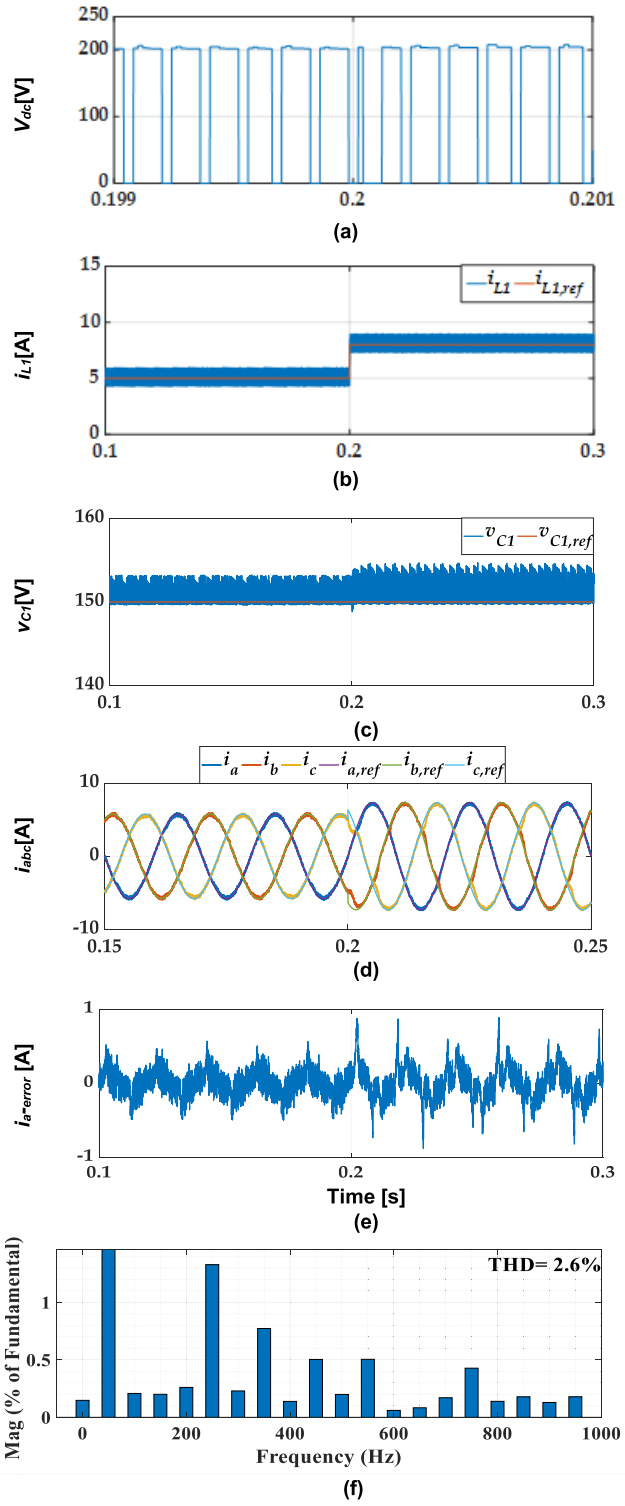

FIGURE 11. Simulation results for the conventional MPC of qZSI.

exhibits improved tracking accuracy with lower output current error than the conventional MPC.

Introducing variable switching frequency is vital in generating a high-quality output current with minimal THD. As depicted in Figures 10(e) and 11(e), the proposed MFPC outperforms the conventional MPC. It demonstrates the smallest error (i_{a_error}) when analyzing the deviation between the measured output current (i_a) and the reference value in phase a ($i_{a,ref}$). This error is quantified as $i_{a\_error} = i_{a\_ref} - i_a$.

In Figures 10(f) and 11(f), the total harmonic distortion (THD) of the output current, as measured in the conventional MPC system, is approximately 2.60%. In contrast, the proposed MFPC demonstrates a substantially lower THD of around 1.64%. This noticeable difference underscores the enhancement of the suggested MFPC system that is provided over the traditional MPC method.

In Figure 12, the output current response to a current reference step is depicted for both the suggested MFPC and the traditional MPC. The illustration clearly shows that the proposed MFPC outperforms the conventional MPC regarding tracking performance, especially in closely following the reference current.

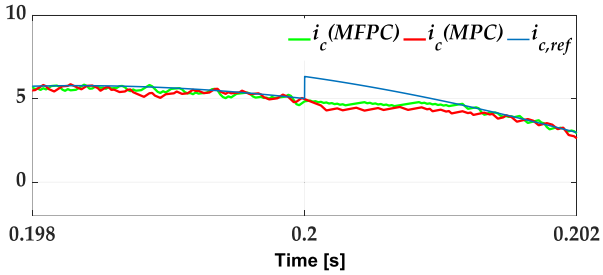

FIGURE 12. The output current of the suggested MFPC and the traditional MPC under the current reference step.

B. SCENARIO 2: LOAD PARAMETERS MISMATCH

A load parameter mismatch is performed for both the conventional MPC and proposed MFPC with qZSI to extend the benchmarking, as illustrated in Figures 13 and 14, respectively. A mismatch between the parameters used in the prediction model and the actual value of the load is introduced. As the instant $t = 200$ ms, the load resistance and inductance values are changed from $R = 12\ \Omega$, $L = 24$ mH to $R = 6\ \Omega$, L=12 mH. As evident, under the same other simulation conditions, the proposed MFPC method demonstrates precise control of the output current compared to the conventional MPC technique. The primary reason for this discrepancy is that the conventional MPC relies on accurate system model parameters. When the model is not precise or contains inaccuracies, the controller's effectiveness is compromised, leading to suboptimal performance.

C. SCENARIO 3: qZSN MODEL MISMATCH

To highlight the proposed MFPC's efficacy in addressing uncertainty, the values of the capacitance and inductance in the qZSI are decreased by 10% in both control systems. The system was subsequently simulated, as depicted in Figures 15 and 16, to showcase the reference and measured currents under inductance and capacitance uncertainties (i.e., -10%). This simulation included a step power change from 500 W to 800 W at $t = 200$ ms. When incorporating uncertainties in both inductance and capacitance in both

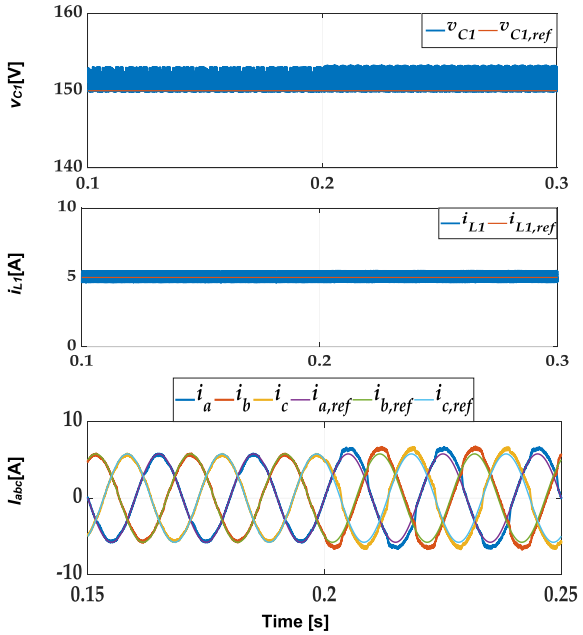

FIGURE 13. The conventional MPC considering *RL* load mismatch.

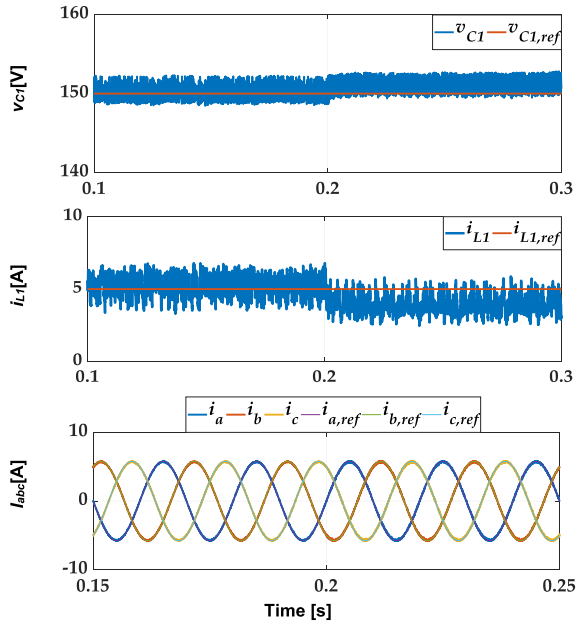

FIGURE 14. The proposed MFPC considering *RL* load mismatch.

control methodologies, no discernible difference is observed between the measured and reference currents after or before the load power variation. In Figures 15 and 16, it is evident that the proposed MFPC outperforms the conventional MPC notably, even in the presence of parameter mismatch and minor errors.

D. SCENARIO 4: THD ASSESSMENT AT INDUCTIVE LOAD MISMATCH

The results depicted in Figure 17 visually highlight the efficacy of the proposed MFPC-based ULM. The proposed MFPC showcases its ability to effectively reject significant

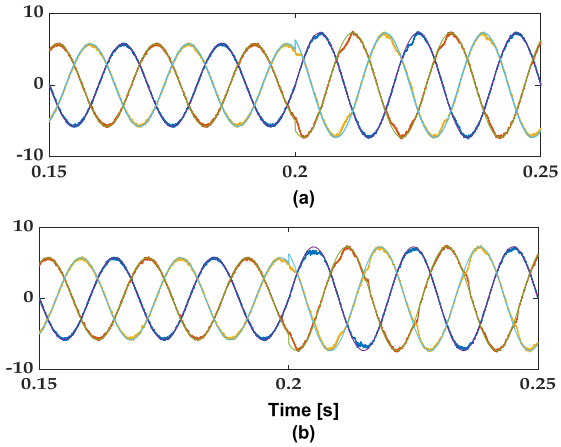

FIGURE 15. Simulated i_{abc} with proposed MFPC under *LC* network mismatch (a) reduce 10% of *C*, (b) reduce 10% of *L*.

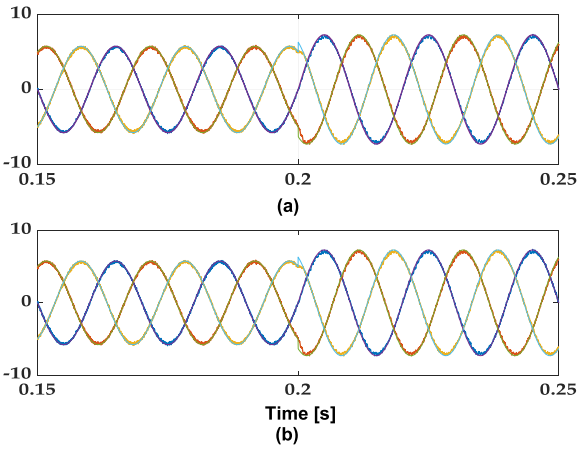

FIGURE 16. Simulated i_{abc} with MPC under *LC* network mismatch (a) reduce 10% of *C*, (b) reduce 10% of *L*.

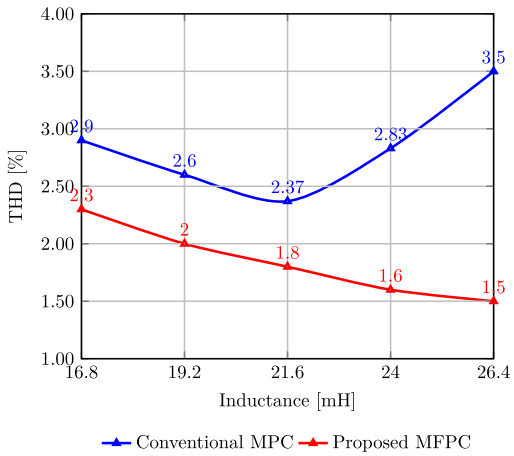

FIGURE 17. Comparison of THD under different *L* values.

changes in filter inductance. This resilience is particularly valuable in dynamic systems where adaptability is crucial.

The use of MFPC implies a reliance on predictive control strategies without the need for an explicit system model, emphasizing the versatility and applicability of the approach.

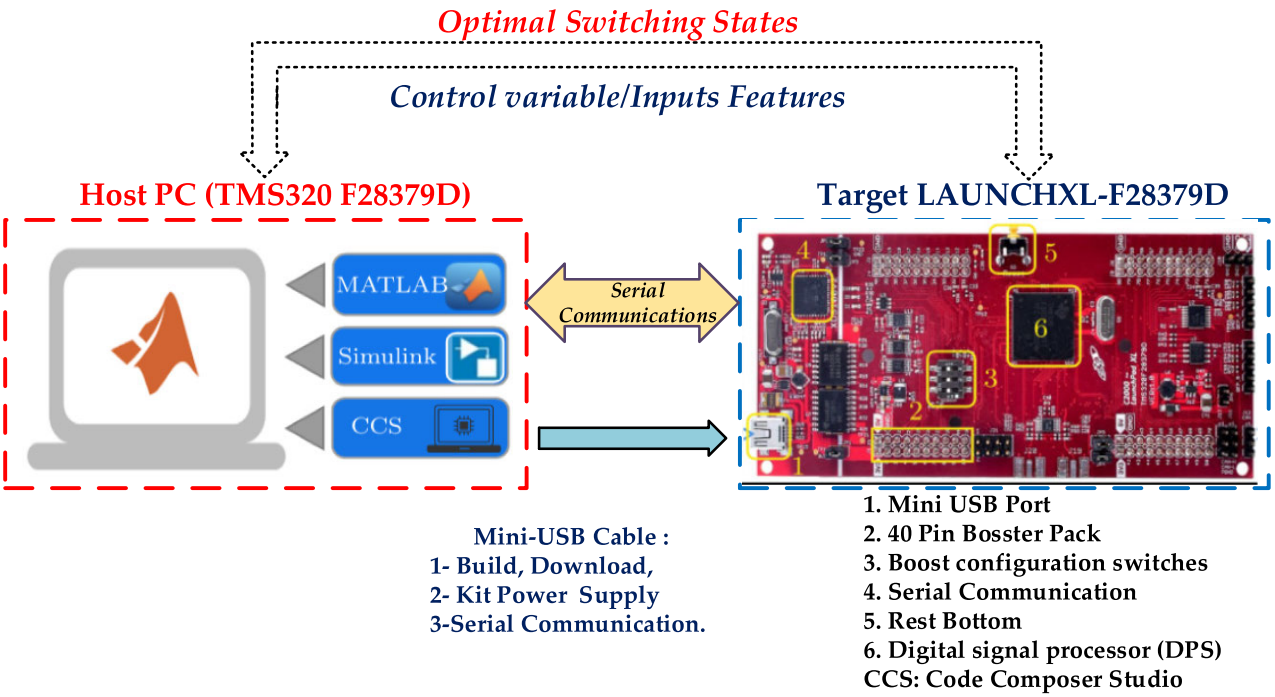

FIGURE 18. Schematic illustration of the HIL implementation for the suggested control setup.

These findings signify a promising advancement, suggesting that the ultra-local model holds potential for practical implementation in scenarios where precise and resilient control amidst variable filter inductance is paramount.

E. SCENARIO 5: THD ASSESSMENT AT VARIOUS SAMPLING PERIODS

The impact of changing the sample time on the operation of the qZSI regulated by the suggested MFPC and the traditional MPC has been investigated. Figure 18 compares the THD of the output voltage of the two controllers at various switching times. THDs with both methods are lower than the recommended values. However, for all sampling periods, the suggested MFPC consistently has the smallest THD.

V. HIL VALIDATION

In this part, we used the HIL validation to verify the practicality of the proposed MFPC using a digital signal processor (DSP) controller. The C2000TM microcontroller LaunchPadXL TMS320F28379D package was created as an HIL emulator to perform tests on the proposed system and investigate simulation findings. In this configuration, the HIL emulator runs a MATLAB model of certain system components, generally the power part, on the computer [29], [30]. This approach allows for testing of the proposed system with accurate simulation representation.

The MATLAB program is a simulation environment, simulating and hosting the proposed system's power components, such as qZSI and load. On the other hand, the microcontroller is implementing the control algorithms, especially those offered by MFPC, into action. Virtual serial COM

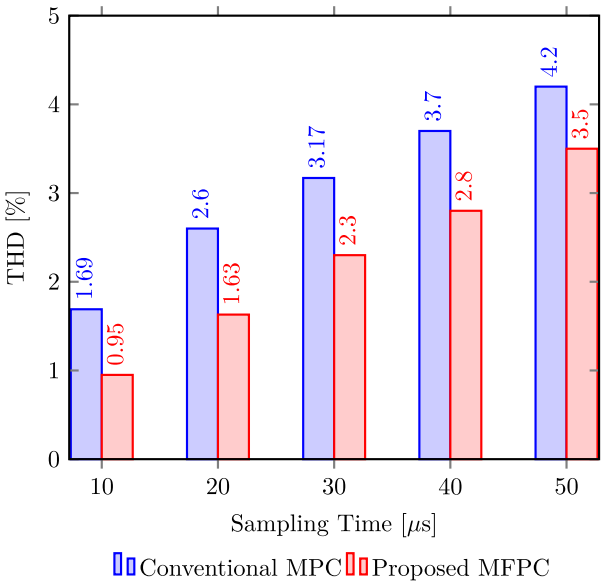

FIGURE 19. THD assessments of the proposed MFPC versus the conventional MPC at various sampling periods.

ports make it easier for the PC and the control board to communicate [31]. As a result, MATLAB could send measured signals from the qZSI circuit to the microcontroller board, such as the v_{dc}, i_{L1}, v_{C1}, and i_{abc}. The microcontroller board generates the qZSI switching signals using the control algorithms. Figure 18 depicts a schematic illustration of the proposed MFPC's HIL implementation, demonstrating how the computational and control components are combined for testing and validation.

TABLE 3. Comparative analysis between the proposed MFPC and the existing models.

Previous work	[32]	[33]	[34]	[35]	[36]	Proposed control
Control strategy	MPC	Direct model predictive current control	MPC current control with phase lock loop	MPC power control	Dual-mode MPC	MFPC
Switching frequency	Variable (20 kHz)	Variable (15 kHz)	Variable (22 kHz)	Constant (10 kHz)	Variable	Variable (9 kHz)
Mismatch parameter test	No	No	No	No	No	Yes
Parameter dependency	Yes	Yes	Yes	Yes	Yes	No
THD (%)	1.9	4	3.2	2.27	2.48	1.2

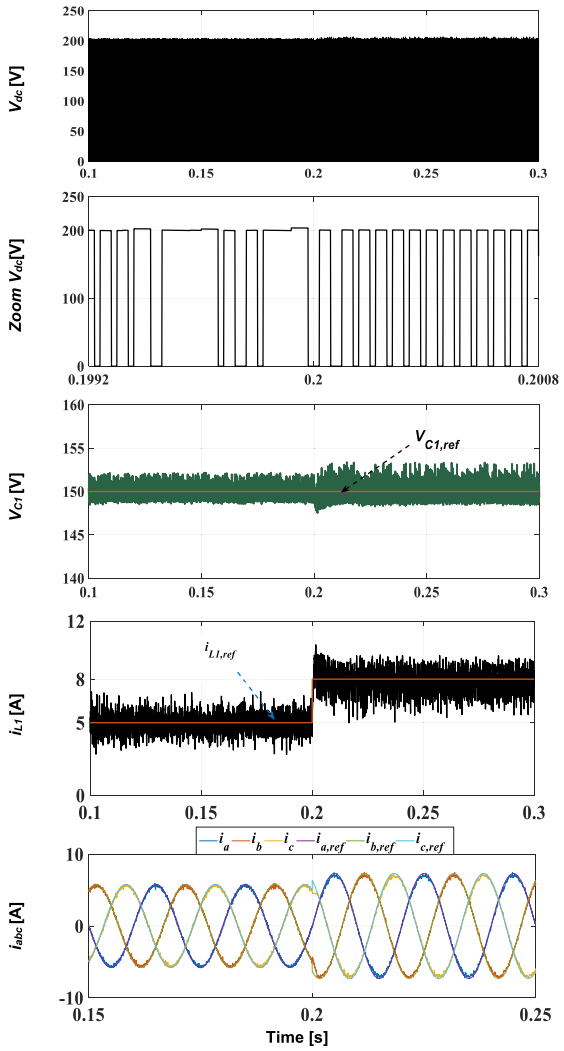

FIGURE 20. The HIL validation of the proposed MFPC under step changes.

Figure 20 displays the outcomes of the HIL validation of the proposed MFPC for the scenario where the desired output power P_{ref} rises from 500 W to 800 W at instant t= 200 ms. Therefore, the peak output current jumps from 5.7 A to 7.3 A. The $i_{L1,ref}$ rises from 5 A to 8 A. The load currents, DC-link voltage, inductor load, and capacitor voltage closely match the simulation results from Figure 11, with some minor deviations due to the measurement noise impacting the waveforms.

It is essential to note that the signals in the HIL implementation exhibit higher noise and spikes compared to the cleaner simulation results of Figure 20. These differences can be attributed to the real-world effects and limitations introduced by the HIL setup, which might lead to minor differences between the HIL validation and simulation results. Nonetheless, the overall concordance between the experimental and simulation findings confirms the efficiency of the suggested MFPC in practice.

VI. COMPARATIVE STUDY

Table 3 provides an insight into the features of switching frequency, line current THD, and other relevant parameters impacted by the proposed MFPC and various control algorithms [32], [33], [34], [35], [36] as assessed through MATLAB simulations. The comparative analysis reveals the discernible advantages of the recommended MFPC, showcasing its capability to enhance line current quality and rectify parameter mismatches.

Unlike some other control methodologies, the MFPC demonstrates robust performance without relying on variations in the qZSI parameters. This unique attribute adds a layer of flexibility to the proposed MFPC, making it a noteworthy consideration in scenarios where parameter independence is a critical factor in the control strategy.

However, it is crucial to highlight a distinctive feature of the proposed MFPC: its independence from the qZSI with the prevalent characteristic of many MPC techniques reliant on cost functions.

VII. CONCLUSION

This work presents a novel model-free control approach, MFPC, for qZSI that can also be applied to other DC/AC single-stage converter configurations. The outcomes demonstrate the benefits of using an MFPC strategy over a conventional MPC, particularly in situations when there are parameter uncertainties or mismatches. The proposed MFPC has the capability to seamlessly integrate the shoot-through state while simultaneously attempting to identify the unknown function in the ULM. The suggested MFPC exhibits excellent performance measurements in both transient and steady modes. It consistently produces favorable results under various operating conditions, including a quick settling time and low output current ripple. In addition, the MFPC approach provides static and dynamic control

effectiveness superior to the conventional MPC technique utilized for benchmarking.

Simulation results further suggest that MFPC can operate effectively without requiring detailed knowledge of the physical model of the qZSI and *RL* load. These findings open up possibilities for exploring the robust application of MFPC in more complex power electronics systems straightforwardly and systematically, paving the way for new avenues of research and practical implementation. Furthermore, experimental confirmation of the suggested MFPC control approach for qZSI is carried out utilizing a DSP controller in the HIL emulator, proving the feasibility and successful execution of the suggested control approach.

REFERENCES

[1] J. Anderson and F. Z. Peng, "Four quasi-Z-source inverters," in *Proc. IEEE Power Electron. Spec. Conf.*, Jun. 2008, pp. 2743–2749.

[2] A. Abid, L. Zellouma, M. Bouzidi, A. Lashab, and B. Rabhi, "Switched inductor Z-source/quasi Z-source network: State of art and challenges," in *Proc. 1st Int. Conf. Commun., Control Syst. Signal Process. (CCSSP)*, May 2020, pp. 477–482.

[3] A. Battiston, E.-H. Miliani, S. Pierfederici, and F. Meibody-Tabar, "Efficiency improvement of a qquasi-Z-source inverter-fed permanent-magnet synchronous machine-based electric vehicle," *IEEE Trans. Transport. Electrific.*, vol. 2, no. 1, pp. 14–23, Mar. 2016.

[4] A. Lashab and D. Sera, "Dual-input quasi-Z-source PV inverter: Dynamic modeling, design, and control," *IEEE Trans. Ind. Electron.*, vol. 67, no. 8, pp. 6483–6493, Aug. 2020.

[5] A. Lashab, D. Sera, J. Martins, and J. M. Guerrero, "Model predictive-based direct battery control in PV fed quasi Z-source inverters," in *Proc. 5th Int. Symp. Environ.-Friendly Energies Appl. (EFEA)*, Sep. 2018, pp. 1–6.

[6] Y. Liu, H. Abu-Rub, and B. Ge, "Z-source/quasi-Z-source inverters: Derived networks, modulations, controls, and emerging applications to photovoltaic conversion," *IEEE Ind. Electron. Mag.*, vol. 8, no. 4, pp. 32–44, Dec. 2014.

[7] W. Liu, Y. Pan, and Y. Yang, "Small-signal modeling and dynamic analysis of the quasi-Z-source converter," in *Proc. 45th Annu. Conf. IEEE Ind. Electron. Soc.*, vol. 1, Oct. 2019, pp. 5039–5044.

[8] H. Rostami and D. A. Khaburi, "Neural networks controlling for both the DC boost and AC output voltage of Z-source inverter," in *Proc. 1st Power Electron. Drive Syst. Technol. Conf. (PEDSTC)*, Feb. 2010, pp. 135–140.

[9] S. Bayhan and H. Komurcugil, "A sliding-mode controlled single-phase grid-connected quasi-Z-source NPC inverter with double-line frequency ripple suppression," *IEEE Access*, vol. 7, pp. 160004–160016, 2019.

[10] A. Bakeer and A. A. Ahmed, "Performance evaluation of PMSM based on model predictive control with field weakening operation and bidirectional quasi Z-source inverter," in *Proc. 19th Int. Middle East Power Syst. Conf. (MEPCON)*, Dec. 2017, pp. 741–746.

[11] A. Lashab, D. Sera, and J. M. Guerrero, "Model predictive control of cascaded multilevel battery assisted quasi Z-source PV inverter with reduced computational effort," in *Proc. IEEE Energy Convers. Congr. Exposit. (ECCE)*, Oct. 2019, pp. 6501–6507.

[12] S. Bayhan, M. Trabelsi, and H. Abu-Rub, "Model predictive control of three-phase three-level neutral-point-clamped qZS inverter," in *Proc. 10th Int. Conf. Compat., Power Electron. Power Eng. (CPE-POWERENG)*, Jun. 2016, pp. 410–415.

[13] A. Abid, A. Bakeer, H. Albalawi, L. Zellouma, M. Bouzidi, A. Lashab, B. Rabhi, and A. Chub, "Optimized modulation scheme for four-leg quasi Z-source inverter: Reducing power loss and improving output quality," *IEEE Access*, vol. 11, pp. 94125–94137, 2023.

[14] Y. Liu, W. Liang, B. Ge, H. Abu-Rub, and N. Nie, "Quasi-Z-source three-to-single-phase matrix converter and ripple power compensation based on model predictive control," *IEEE Trans. Ind. Electron.*, vol. 65, no. 6, pp. 5146–5156, Jun. 2018, doi: 10.1109/TIE.2017.2752122.

[15] A. Bakeer, M. A. Ismeil, and M. Orabi, "A powerful finite control set-model predictive control algorithm for quasi Z-source inverter," *IEEE Trans. Ind. Informat.*, vol. 12, no. 4, pp. 1371–1379, Aug. 2016, doi: 10.1109/TII.2016.2569527.

[16] P. Karamanakos, A. Ayad, and R. Kennel, "A variable switching point predictive current control strategy for quasi-Z-source inverters," *IEEE Trans. Ind. Appl.*, vol. 54, no. 2, pp. 1469–1480, Mar. 2018, doi: 10.1109/TIA.2017.2765302.

[17] Y. Xu, Y. He, and S. Li, "Logical operation-based model predictive control for quasi-Z-source inverter without weighting factor," *IEEE J. Emerg. Sel. Topics Power Electron.*, vol. 9, no. 1, pp. 1039–1051, Feb. 2021, doi: 10.1109/JESTPE.2020.2973183.

[18] Y. Liu, H. Abu-Rub, Y. Xue, and F. Tao, "A discrete-time average model-based predictive control for a quasi-Z-source inverter," *IEEE Trans. Ind. Electron.*, vol. 65, no. 8, pp. 6044–6054, Aug. 2018.

[19] Y. Xu and H. Xiao, "Combinative voltage vector-based model predictive control for performance improvement of quasi Z-source inverter," *IEEE Access*, vol. 9, pp. 143013–143025, 2021, doi: 10.1109/ACCESS.2021.3121019.

[20] A. Mahmoudi, I. Jlassi, A. J. M. Cardoso, and K. Yahia, "Model free predictive current control based on a grey wolf optimizer for synchronous reluctance motors," *Electronics*, vol. 11, no. 24, p. 4166, Dec. 2022.

[21] Y. Zhang, T. Jiang, and J. Jiao, "Model-free predictive current control of a DFIG using an ultra-local model for grid synchronization and power regulation," *IEEE Trans. Energy Convers.*, vol. 35, no. 4, pp. 2269–2280, Dec. 2020.

[22] J. Rodríguez, R. Heydari, Z. Rafiee, H. A. Young, F. Flores-Bahamonde, and M. Shahparasti, "Model-free predictive current control of a voltage source inverter," *IEEE Access*, vol. 8, pp. 211104–211114, 2020.

[23] M. Khalilzadeh, S. Vaez-Zadeh, J. Rodriguez, and R. Heydari, "Model-free predictive control of motor drives and power converters: A review," *IEEE Access*, vol. 9, pp. 105733–105747, 2021.

[24] A. Bakeer, G. Magdy, A. Chub, F. Jurado, and M. Rihan, "Optimal ultra-local model control integrated with load frequency control of renewable energy sources based microgrids," *Energies*, vol. 15, no. 23, p. 9177, Dec. 2022.

[25] X. Sun, J. Cao, G. Lei, Y. Guo, and J. Zhu, "A robust deadbeat predictive controller with delay compensation based on composite sliding-mode observer for PMSMs," *IEEE Trans. Power Electron.*, vol. 36, no. 9, pp. 10742–10752, Sep. 2021.

[26] Y. Zhang, J. Jiao, and J. Liu, "Direct power control of PWM rectifiers with online inductance identification under unbalanced and distorted network conditions," *IEEE Trans. Power Electron.*, vol. 34, no. 12, pp. 12524–12537, Dec. 2019.

[27] M. Kermadi, A. Rebai, L. Baghli, N. Mesbahi, S. Mekhilef, and M. Mubin, "A model-free predictive current controller for voltage source inverters," Tech. Rep.

[28] M. Fliess and C. Join, "Model-free control," *Int. J. Control*, vol. 86, no. 12, pp. 2228–2252, 2013.

[29] H. Albalawi, A. Bakeer, S. A. Zaid, E.-H. Aggoune, M. Ayaz, A. Bensenouci, and A. Eisa, "Fractional-order model-free predictive control for voltage source inverters," *Fractal Fractional*, vol. 7, no. 6, p. 433, May 2023, doi: 10.3390/fractalfract7060433.

[30] S. A. Zaid, I. S. Mohamed, A. Bakeer, L. Liu, H. Albalawi, M. E. Tawfiq, and A. M. Kassem, "From MPC-based to end-to-end (E2E) learning-based control policy for grid-tied 3L-NPC transformerless inverter," *IEEE Access*, vol. 10, pp. 57309–57326, 2022, doi: 10.1109/ACCESS.2022.3173752.

[31] A. Abid, A. Bakeer, L. Zellouma, M. Bouzidi, A. Lashab, and B. Rabhi, "Low computational burden predictive direct power control of quasi Z-source inverter for grid-tied PV applications," *Sustainability*, vol. 15, no. 5, p. 4153, Feb. 2023.

[32] M. Mosa, R. S. Balog, and H. Abu-Rub, "High-performance predictive control of quasi-impedance source inverter," *IEEE Trans. Power Electron.*, vol. 32, no. 4, pp. 3251–3262, Apr. 2017, doi: 10.1109/TPEL.2016.2531989.

[33] A. Ayad, P. Karamanakos, and R. Kennel, "Direct model predictive current control strategy of quasi-Z-source inverters," *IEEE Trans. Power Electron.*, vol. 32, no. 7, pp. 5786–5801, Jul. 2017, doi: 10.1109/TPEL.2016.2610459.

[34] S. Jain, M. B. Shadmand, and R. S. Balog, "Decoupled active and reactive power predictive control for PV applications using a grid-tied quasi-Z-source inverter," *IEEE J. Emerg. Sel. Topics Power Electron.*, vol. 6, no. 4, pp. 1769–1782, Dec. 2018, doi: 10.1109/JESTPE.2018.2823904.

[35] X. Duan, L. Kang, H. Zhou, and Q. Liu, "Multivector model predictive power control with low computational burden for grid-tied quasi-Z-source inverter without weighting factors," *IEEE Trans. Power Electron.*, vol. 37, no. 10, pp. 11739–11748, Oct. 2022, doi: 10.1109/TPEL.2022.3174303.

[36] S. Sajadian and R. Ahmadi, "Model predictive control of dual-mode operations Z-source inverter: Islanded and grid-connected," *IEEE Trans. Power Electron.*, vol. 33, no. 5, pp. 4488–4497, May 2018.

ABDERAHMANE ABID was born in Taibet, Algeria, in 1988. He received the bachelor's degree in electrical engineering from Boumerdes University, Algeria, in 2012, and the master's degree in electrical engineering from the University of Ouargla, in 2015. He is currently pursuing the Ph.D. degree in electrical energy with the University of El Oued. His research interests include impedance source converters, microgrids, and photovoltaic applications.

ABUALKASIM BAKEER (Senior Member, IEEE) was born in Qena, Egypt, in 1990. He received the B.Sc. and M.Sc. (Hons.) degrees in electrical engineering from Aswan University, Egypt, in 2012 and 2017, respectively, and the Ph.D. degree in electrical engineering from Tallinn University of Technology, Tallinn, Estonia, in June 2023.

In 2014, he joined the Electrical Engineering Department, Faculty of Engineering, Aswan University, Aswan, Egypt, first as a Demonstrator and then as an Assistant Lecturer, in 2017. He is currently a Postdoctoral Fellow with the Department of Electrical Power Engineering and Mechatronics, Tallinn University of Technology. He is the author or coauthor of over 70 scientific articles. He is also the coauthor of one book chapter about shade-tolerant PV microconverters. His main research interests include dc–dc converters, fault diagnosis and fault tolerance, impedance-source power converters, model predictive control, applications of neural networks in power electronics, and renewable energy integration. He serves as a Reviewer for several prestigious journals, such as IEEE TRANSACTIONS ON INDUSTRIAL ELECTRONICS, IEEE TRANSACTIONS ON INDUSTRIAL INFORMATICS, IEEE JOURNAL OF EMERGING AND SELECTED TOPICS IN INDUSTRIAL ELECTRONICS, and *ISA Transactions*.

HANI ALBALAWI received the B.Sc. degree in electrical engineering from King Abdulaziz University, Jeddah, Saudi Arabia, in 2008, the M.S. degree in automatic control system engineering from The University of Sheffield, Sheffield, U.K., in 2011, and the Ph.D. degree from Clemson University, Clemson, SC, USA, in 2016. He is currently a Faculty Member with the Department of Electrical Engineering, Faculty of Engineering. His research interests include renewable energy, energy management, energy storage, power system quality, power system planning and operation, and power system control.

MANSOUR BOUZIDI (Member, IEEE) was born in M'sila, Algeria, in 1985. He received the engineering degree in electrical engineering from M'sila University, M'sila, in 2009, and the M.S. and Ph.D. degrees in power electronics from Djillali Liabes University, Sidi-Bel-Abbes, Algeria, in 2011 and 2017, respectively. Since 2012, he has been an Associate Professor with the University of Ouargla, Ouargla, Algeria. His current research interests include power electronics, renewable energy conversion, and electrical drives.

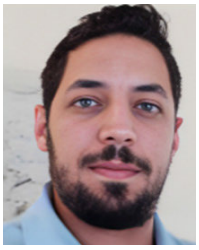

ABDEREZAK LASHAB (Senior Member, IEEE) received the Baccalaureate degree (Hons.) from the High School, Cheikh Ibrahim Bayoud, Constantine, Algeria, in 2007, the bachelor's and master's degrees in electrical engineering from the Université des Frères Mentouri Constantine 1, Constantine, in 2010 and 2012, respectively, and the Ph.D. degree in developing and investigating new converter topologies and control methods of photovoltaic systems with and without storage from the Department of Energy Technology, Aalborg University, Denmark, in 2019.

From 2012 to 2013, he was an Engineer with High Tech Systems (HTS). From 2013 to 2016, he was a Research Assistant with the Université des Frères Mentouri Constantine 1, where he helped teach several electrical engineering courses for undergraduate students. From April 2019 to July 2019, he was a Visiting Researcher with the Chair of Power Electronics, Kiel University, Germany. He is currently a Postdoctoral Researcher with Aalborg University. His current research interests include power electronics topologies, modeling, and control for photovoltaic systems with and without storage. He serves as a Reviewer for IEEE TRANSACTIONS ON INDUSTRIAL ELECTRONICS, IEEE TRANSACTIONS ON POWER ELECTRONICS, IEEE TRANSACTIONS ON INDUSTRIAL INFORMATICS, IEEE TRANSACTIONS ON SUSTAINABLE ENERGY, *IET Power Electronics*, *IET Electronics Letters*, and several IEEE conferences.

ANDRII CHUB (Senior Member, IEEE) received the B.Sc. and M.Sc. degrees in electronic systems from Chernihiv State Technological University, Ukraine, in 2008 and 2009, respectively, and the Ph.D. degree in electrical engineering from Tallinn University of Technology, Tallinn, Estonia, in 2016. He was a Visiting Research Fellow with Kiel University, in 2017, and a Postdoctoral Researcher with Federico Santa Maria Technical University, from 2018 to 2019. He is currently a Senior Researcher with the Power Electronics Group, Department of Electrical Power Engineering and Mechatronics, Tallinn University of Technology. He has coauthored more than 100 articles and a book chapter on power electronics and applications and holds several patents and utility models. His research interests include advanced dc–dc converter topologies, renewable energy conversion systems, energy-efficient buildings, reliability, and fault-tolerance of power electronic converters. He has received numerous best paper awards at IEEE conferences and the IEEE Industrial Electronics Society Best Conference Paper Award, in 2018. He is an Associate Editor of IEEE JOURNAL OF EMERGING AND SELECTED TOPICS IN INDUSTRIAL ELECTRONICS.

SHERIF A. ZAID was born in Cairo, Egypt, in 1970. He received the B.Sc., M.Sc., and Ph.D. degrees in electrical engineering from the Faculty of Engineering, Cairo University, Giza, Egypt, in 1992, 1996, and 2001, respectively. Since 2017, he has been a Full Professor of power electronics with the Department of Electrical Power, Faculty of Engineering, Cairo University. He has published around 60 research articles and participated in many research projects. His research interests include power electronics, renewable energy systems, and electrical drives. He is a reviewer of many reputable journals.